ACS OMEGA

http://pubs.acs.org/journal/acsodf

Article

Dynamic Model of the Short-Term Synaptic Behaviors of PEDOT-based Organic Electrochemical Transistors with Modified Shockley Equations

Haonian Shu, Haowei Long, Haibin Sun, Baochen Li, Haomiao Zhang, and Xiaoxue Wang*

Cite This: *ACS Omega* 2022, 7, 14622−14629

Read Online

ACCESS | Metrics & More | Article Recommendations | Supporting Information

ABSTRACT: Neuromorphic computing is an emerging area with prospects to break the energy efficiency bottleneck of artificial intelligence (AI). A crucial challenge for neuromorphic computing is understanding the working principles of artificial synaptic devices. As an emerging class of synaptic devices, organic electrochemical transistors (OECTs) have attracted significant interest due to ultralow voltage operation, analog conductance tuning, mechanical flexibility, and biocompatibility. However, little work has been focused on the first-principal modeling of the synaptic behaviors of OECTs. The simulation of OECT synaptic behaviors is of great importance to understanding the OECT working principles as neuromorphic devices and optimizing ultralow power consumption neuromorphic computing devices. Here, we develop a two-dimensional transient drift−diffusion model based on modified Shockley equations for poly(3,4-ethylenedioxythiophene) (PEDOT)-based OECTs. We reproduced the typical transistor characteristics of these OECTs including the unique non-monotonic transconductance−gate bias curve and frequency dependency of transconductance. Furthermore, typical synaptic phenomena, such as excitatory/inhibitory postsynaptic current (EPSC/IPSC), paired-pulse facilitation/depression (PPF/PPD), and short-term plasticity (STP), are also demonstrated. This work is crucial in guiding the experimental exploration of neuromorphic computing devices and has the potential to serve as a platform for future OECT device simulation based on a wide range of semiconducting materials.

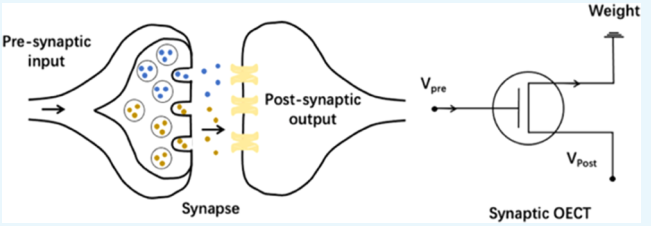

INTRODUCTION

The rapidly developing artificial intelligence (AI) is pushing the traditional von Neumann computational architecture to its energy efficiency limit.[1] In the von Neumann architecture, the dynamic random access memory (DRAM) and the processing units are separated physically, resulting in immense energy consumption associated with data movement.[2,3] On the contrary, in human brains, massive information can be processed in parallel in memory at an extremely fast speed with a super low power consumption of merely 1−100 fJ per synapse.[4,5] Inspired by human brains, the emerging neuromorphic computing has attracted massive research interest. A key component for neuromorphic computing and artificial neural networks is artificial synapses.[6] Emulating biological synapses, an artificial synapse responds to stimuli of action potential spikes with programmed postsynaptic current by modulating the device conductance.[7] Recently, different synaptic functions such as short-term plasticity (STP),[8] long-term potentiation,[9,10] and spike-timing-dependent plasticity (STDP)[11] have been achieved by organic and inorganic artificial synaptic devices. Massive research effort are put into the materials selection for synaptic transistors, including zero-dimensional (0D) quantum dots,[12−14] one-dimensional (1D) nanostructure,[15−18] two-dimensional (2D) nanostructures,[19−22] three-dimensional (3D) architectures,[23−25] transition-metal oxide,[26] ferroelectric materials,[27,28] alloy,[29] mixed structure,[30−32] and organic materials.[33,34] Among the artificial synaptic devices, synapses based on organic electrochemical transistors (OECTs, Figure 1A−C) have emerged as attractive alternatives to inorganic counterparts owing to their fast response speed,[35] high transconductance,[36] less stochastic writing,[2] continuous conductance tuning,[37] and low driving voltage comparable to biological synapses.[38] A schematic representation of an OECT synapse is shown in Figure 1D. The phosphate-buffered saline (PBS) electrolyte together with a gold gate electrode of an OECT transmits a presynaptic signal, while the PEDOT: polystyrene sulfonate (PSS) channel together with the source and drain electrodes transmits a postsynaptic output signal in the form of source−drain current (I_{ds}). The experimental work has demonstrated that OECTs have synaptic functionalities like spike-timing-dependent

Received: December 4, 2021
Accepted: April 7, 2022
Published: April 19, 2022

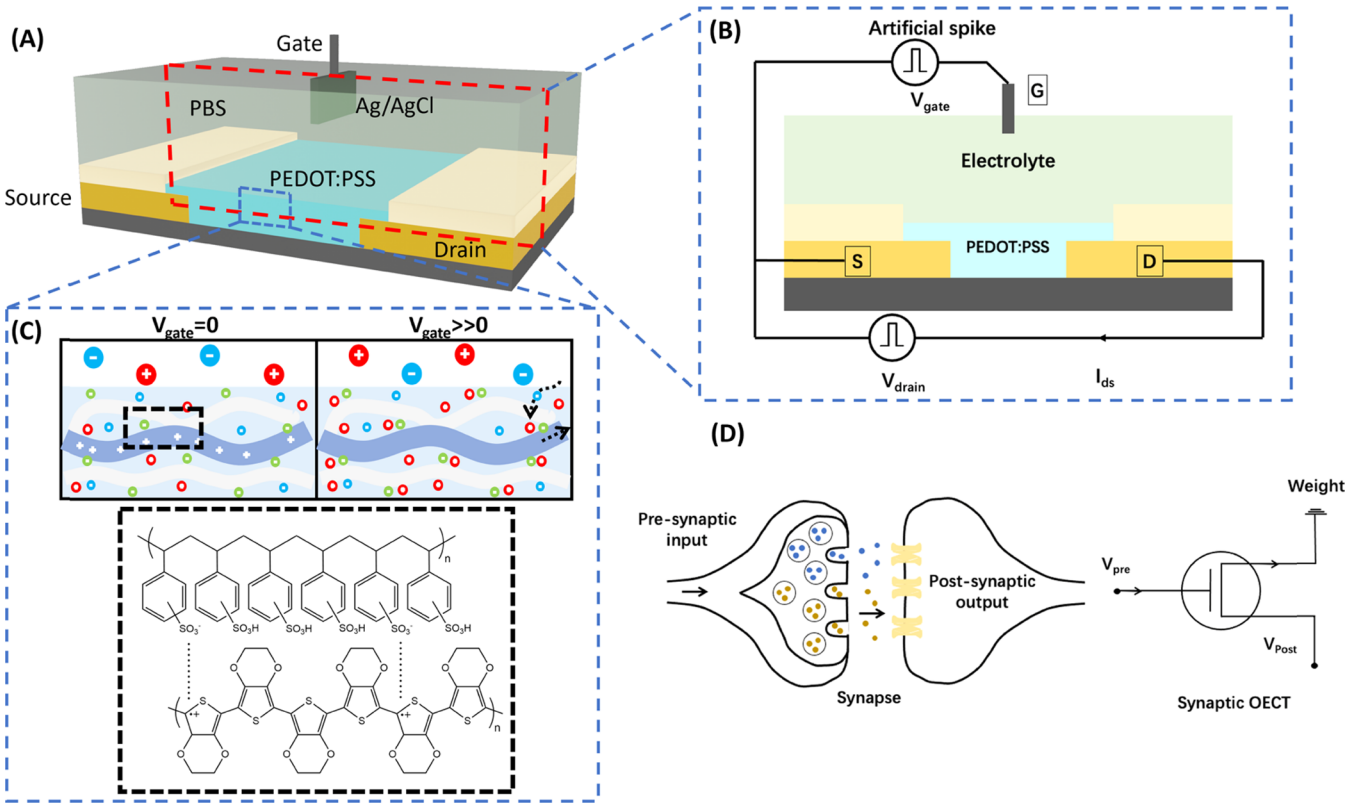

Figure 1. Device apparatuses and phase separation. (A) Sketch of an electrolyte-gated PEDOT:PSS OECT. Adapted from ref 19. (B) 2D overview of the synaptic OECT. The essential components are a PEDOT:PSS channel with gold source and drain contact, an electrolyte, and an Ag/AgCl gate electrode. (C) Schematic demonstration of phase separation in PEDOT:PSS. The blue part stands for the PEDOT phase, while the gray parts stand for the PSS phase. When $V_{gate} = 0$, PEDOT:PSS is doped, $I_{ds} > 0$, when $V_{gate} \gg 0$, OECT is in depletion mode, PEDOT:PSS is de-doped, carrier density in the polymer film decreases, $I_{ds} = 0$. The polarons in the PEDOT phase are stabilized by immobilized counterions in the PSS phase. (D) Schematic representation of the synaptic OECT in analogy to a biological synapse.

plasticity and homeostatic plasticity.[39,40] However, theoretical understanding of the working principles of OECT-type artificial synapses is still in its very early stage.

Theoretical modeling of OECT synaptic performances is crucial since it does not only allow us to understand the working principles of OECT as neuromorphic devices but also guides future experiments. In an OECT (Figure 1A), an applied potential on the gate drives ions from the electrolyte into the polymer channel, changing its redox state and conductivity as a result. Typically, there are two types of device modes for OECTs: the depletion mode and the accumulation mode.[41] In the depletion mode, the channel material is fully oxidized (heavily p-doped) such as PEDOT:PSS (the case illustrated in Figure 1A,B). When a positive gate potential is applied, cations are injected from the electrolyte into the channel; as a result, the holes in the channel are depleted and the conductance of the channel is dropped (Figure 1C). In the accumulation mode, the channel materials are usually nearly intrinsic semiconducting polymers with a very small number of mobile holes. When a negative gate potential is applied, anions are injected into the channel and electrochemical doping is induced. Therefore, the channel conductance increases. The change in channel conductance is typically transient or volatile in OECTs, meaning that the conductance returns to its initial value after the applied gate voltage is removed. The volatile conductance tuning is essential for short-term synaptic behaviors in OECT-based artificial synapses. The short-term synaptic behaviors are essential for critical computational functions such as signal transmission, encoding, and filtering of neuronal signals.[3,6]

Modeling the synaptic behaviors of OECT-based artificial synapses has been a crucial yet long existing challenge for the field of neuromorphic computing. The fundamental equations used to describe the charge-carrier and ion transport process in OECTs include the Poisson equation, the drift−diffusion equation for electronic charge-carrier transport, and the drift−diffusion equation for ion transport. These equations are analogous to the well-known Shockley equations[42] for modeling electron and hole transport in semiconductor devices such as p−n junction diodes and metal-oxide semiconductor field-effect transistors (MOSFETs). Efforts have been put into modifying and solving the Shockley equations, which would provide physical insight into the system. Shirinskaya et al. described the doping−de-doping interface as the moving front, based on which a numerical model for the current−voltage characteristics of OECTs was developed.[43] Tybrandt et al. proposed a time-dependent approach based on the drift−diffusion−Poisson equation and phase separation. Their model successfully describes the experimental data. The model though is limited to one-dimensional (1D) across channel and electrolyte and does not reflect neuromorphic behavior. The frequency dependency of transconductance and the unique bell-shaped transconductance−gate bias curve are also not reproduced by their model.[44] The experimental and modeling results of Volkov et al. provide a solid argument that the major contribution to the capacitance of the two-phase

https://doi.org/10.1021/acsomega.1c06864
ACS Omega 2022, 7, 14622−14629

PEDOT:PSS originates from electric double layers (EDLs) formed along the interfaces between the PEDOT-rich region and the PSS-rich region.[45] However, limited work has been done on modeling the artificial synaptic behaviors of OECTs. The key challenge of this task is that there is still a lack of 2D dynamic models of the cross section of OECT describing the complex electrochemical processes in OECT synaptic tuning, which provides a deeper perspective on the working principles of OECTs. At the same time, understanding the electronic structure of semiconducting polymers is also essential for modeling key synaptic behaviors of OECTs.

To address this key challenge, we adopted the concept of PEDOT and PSS phase separation and built a 2D transient model for the prototype depletion-mode OECT and demonstrated OECT transistor characteristics and synaptic behaviors with a modified Shockley equation model for the first time. Typical OECT transistor behaviors such as transfer characteristics, output characteristics, and a small signal transconductance are reproduced. In addition, the bell-shaped transconductance−gate bias curve is reproduced by assuming a Gaussian-shaped density of states (DOS) in the organic semiconductor.[44,46] The frequency dependency of transconductance is also studied using our 2D dynamic model, demonstrating the physical validity of our model.[47−49] Moreover, synaptic behaviors, such as excitatory/inhibitory postsynaptic current (EPSC/IPSC), paired-pulse facilitation/depression (PPF/PPD), short-term plasticity (STP), spike-amplitude-dependent plasticity (SADP), spike-duration-dependent plasticity (SDDP), are achieved. This work lays the foundations for the simulation of large-scale programmable and functional neuromorphic arrays for energy-efficient computing. In addition, this work will provide a modular platform for the design of novel OECT synaptic devices.

RESULTS AND DISCUSSION

Model Description. In the Bernards model,[50] the OECTs are considered as consisting of two circuits: the ionic circuit, where ions are transported in the polyelectrolyte blends, and the electronic circuit, where holes are transported on the conjugated polymer backbone. Based on this idea, Tybrandt et al.[44] treated these two phases distinctively in a classic PEDOT:PSS system: the electronic conjugated polymer (PEDOT, CP) phase and the ionic polyelectrolyte (PSS, PE) phase (Figure 1C). Typical OECT characteristics such as transfer characteristics and output characteristics, along with charging characteristics, are reproduced by considering the drift−diffusion for both electronic and ionic carriers and the effect of EDL capacitance between these two phases in a 1D model. Recently, Paulsen et al.[51] brought up the concept of organic mixed ionic−electronic conductors (OMIEC) for an efficient description of not only ionic and electronic transport but more importantly ionic−electronic coupling. PEDOT:PSS, as the OMIEC, and OECTs, as a typical configuration of OMIEC devices, allows the adaption of the OMIEC concept in our model.

In our work, we extended the prototypical model based on the Shockley equations to two dimensions with a focus on transient behaviors. PEDOT:PSS is a classic two-component OMIEC with anions chemically linked to the PSS component. The electronic transport mechanism in the PEDOT phase should contain both thermally activated hopping and band-like transport, depending on its crystallinity.[52] In our model, it is described by a classical drift−diffusion equation modified by electrochemical potential with the unit of energy (μ_p) (eq 1), where p is the hole concentration, D_p is the diffusion coefficient of holes in PEDOT, and f is F/RT, which is the ratio between Faraday's constant and RT according to the Einstein relation, and $\vec{j}_p$ is the flux of holes. By assuming Gaussian density of states (DOS), the chemical potential can be modified as eq 2, where E_{DOS} is the center energy of the Gaussian DOS, σ is the standard deviation of the DOS and is a measure of the energetic disorder, p_t is the total available hole density, and B is defined as eq 3.

$$\overrightarrow{j_p} = -D_p(\vec{\nabla}p + fp\vec{\nabla}(V_p + \mu_p/e)) \quad (1)$$

$$\mu_p = k_B T \ln(p) + eB \quad (2)$$

$$B = \left(E_{DOS} - \frac{\sigma^2}{2k_B T} - k_B T \ln(p_t)/e\right) \quad (3)$$

Similarly, the ionic transport in the PE phase follows a hopping mechanism, which is described by the classic drift−diffusion equation (eq 4), where $\overrightarrow{j_{c_\pm}}$ is the flux of cations and anions, respectively. $c_\pm$ is the concentration of cations and anions, respectively. Because of phase separation, the electrostatic potential in these two phases is distinctly labeled as V_p for the CP phase and V_c for the PE phase.

$$\overrightarrow{j_{c_\pm}} = -D_{c_\pm}(\vec{\nabla}c_\pm \pm fc_\pm\vec{\nabla}V_c) \quad (4)$$

At the interface between phase separating regions, the spatial separation between the electronic and ionic charge carriers causes the formation of EDLs. This process exists throughout the system, which enables us to consider this process as a volumetric property when viewed from a macroscopic level. This volumetric capacitance of EDL is labeled as C_V. Continuity equations (eqs 5 and 6) and Poisson's equation (eq 7) are implemented to relate charge-carrier concentration to flux densities. It is assumed that holes that compensate for negative ionic charges in EDL do not contribute to Poisson's equation (eq 8).

$$\vec{\nabla}\cdot\overrightarrow{j_p} + \partial p/\partial t = 0 \quad (5)$$

$$\vec{\nabla}\cdot\overrightarrow{j_{c_\pm}} + \partial c_\pm/\partial t = 0 \quad (6)$$

$$-\varepsilon\vec{\nabla}^2 V_c/F = p + c_+ - c_- - c_{fix} \quad (7)$$

$$-\varepsilon\vec{\nabla}V_p/F = p - (V_p - V_c)C_V \quad (8)$$

Boundary conditions are adapted from Tybrandts' model considering the continuity of Fermi level and charge neutrality at the PEDOT−electrode interface. Full sets of the drift−diffusion equations and boundary conditions are shown in Figure S1. The presence of net ionic charge in the PE phase leads to the presence of electronic charge in an OMIEC of the opposite sign. The balancing process of excess ionic charge with electronic charge is called electrochemical doping as it causes an increase in the electrical conductivity in the OMIEC. In PEDOT:PSS, stabilizing ionic charge is immobilized in the PE phase, thus it is inherently doped.

Transistor Characteristics. Unless specified otherwise, the parameters used in all of the calculations are shown in Table

https://doi.org/10.1021/acsomega.1c06864
ACS Omega 2022, 7, 14622−14629

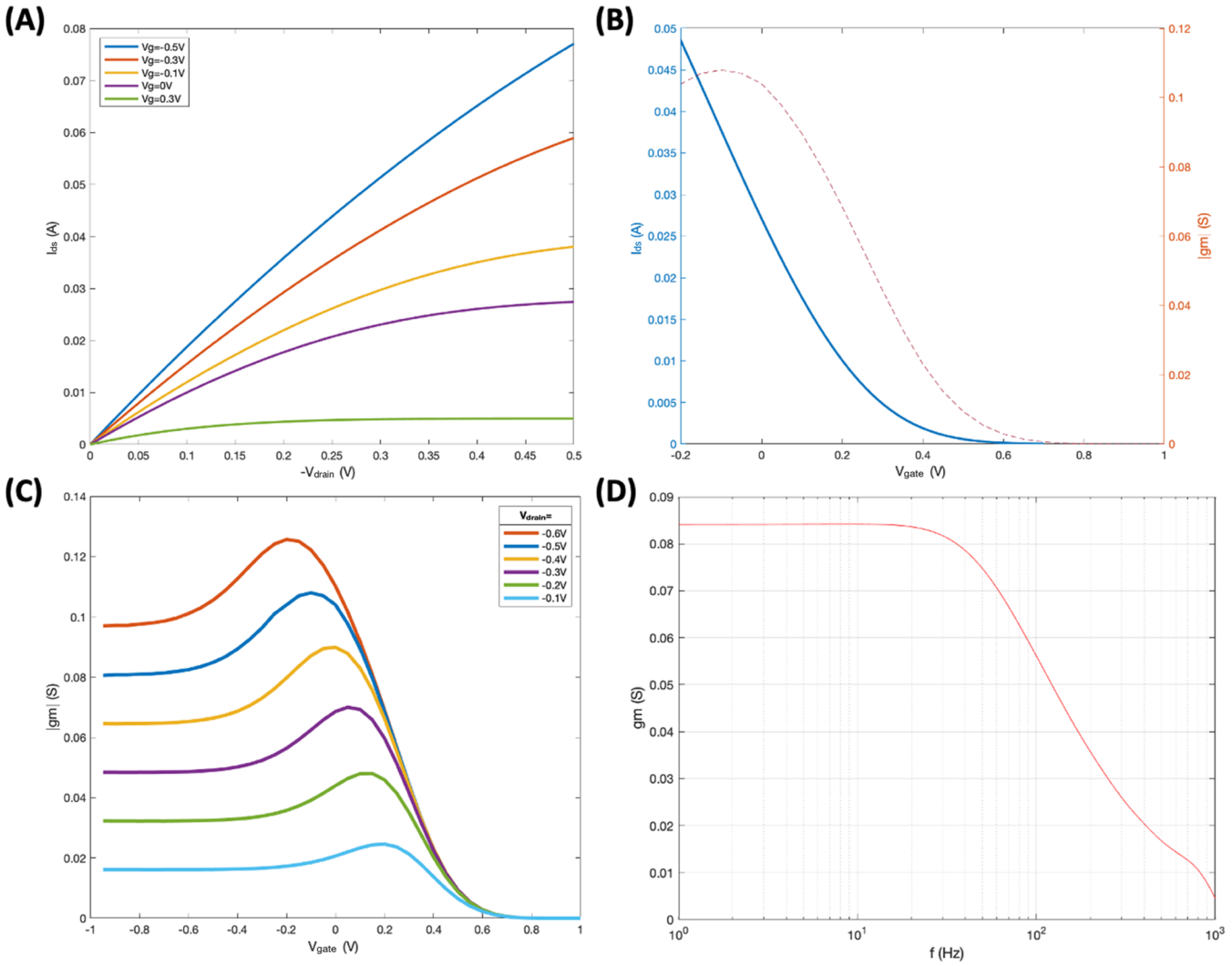

Figure 2. Simulation results of transistor characteristics. (A) Output characteristics of V_{gate} vary from −0.5 V (top curve) to 0.3 V (bottom curve). (B) Transfer characteristics and the associated transconductance for V_{drain} = −0.5 V. (C) Steady-state transconductance. (D) Frequency response of the transconductance.

S1. One can refer to Figure S3 for the dimensions and mesh in the simulations for a single transistor with channel length L = 200 μm and channel thickness W = 10 μm. The current density is obtained by integrating all charge-carrier species flux throughout the channel on the cross-sectional area. Similarly, the current density in the electrolyte (I_g) can also be calculated by integrating ionic carriers throughout the cross-sectional area in the electrolyte.

As shown in Figure 2, typical transistor characteristics of OECTs are qualitatively reproduced.[36] The output characteristics in Figure 2A are qualitatively in good agreement with typical PEDOT:PSS-based OECTs, where I_{ds} initially increases as V_{drain} decreases and then reaches a plateau. Higher V_{gate} requires less negative V_{drain} to reach a plateau and results in a lower drain current. The transfer characteristics and the associated transconductance (g_m) in Figure 2B also align with the typical PEDOT:PSS-based OECTs.[47] I_{ds} reaches a maximum plateau as V_{gate} decreases and a minimum plateau as V_{gate} increases. The transconductance has a non-monotonic dependence on gate voltage,[53,54] which is a unique characteristic for OECTs and agrees with the convex-shaped transconductance curve in Figure 2B,C. The non-monotonic transconductance is an intrinsic property of OECTs. This happens because of the behavior of holes filling the DOS in PEDOT as the gate voltage gets lower, assuming a Gaussian DOS. When the DOS is much less than half-full, both hole concentration and hole mobility increase with increasing holes, thus transconductance increases as gate voltage becomes more negative. When the DOS is nearly half-full, the rate of increase of hole concentration and hole mobility slows with increasing holes. As a result, transconductance decreases with a more negative gate voltage. When DOS is more than half-full, adding holes leads to a decrease in hole mobility, resulting in a negative transconductance.[47]

The frequency response in Figure 2D is obtained by measuring the small signal transconductance. A 100 mV oscillation is applied on the gate electrode and the transconductance is determined by the amplitude ratio between output I_{ds} oscillation and the corresponding gate bias. This behavior is in agreement with the fact that typical OECTs have higher transconductances, in the range of millisiemens, and can only operate at lower frequencies compared to organic field-effect transistors (OFETs).[41]

https://doi.org/10.1021/acsomega.1c06864
ACS Omega 2022, 7, 14622−14629

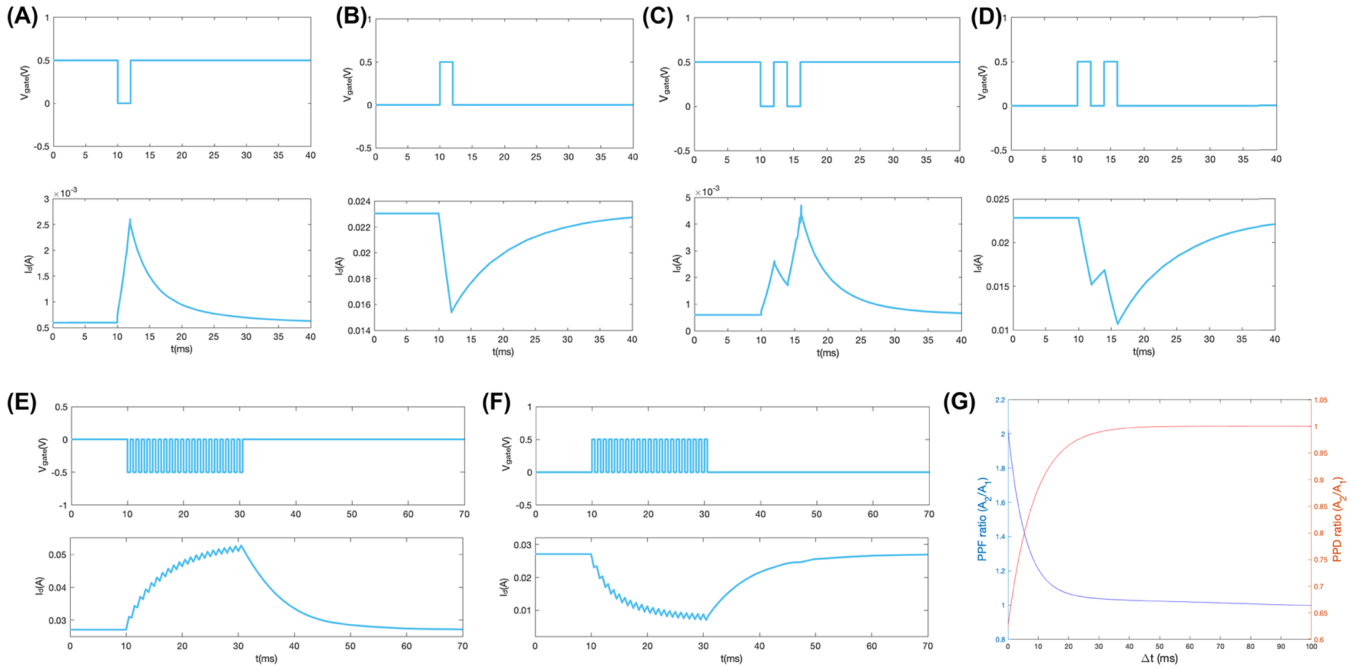

Figure 3. Simulation results of typical OECT synaptic behaviors. (A) EPSC triggered by a postsynaptic pulse (V_{pre} = 0.5 *V*, V_{post} = 0 V, t_d = 2 ms, V_{drain} = −0.3 V). (B) IPSC triggered by a presynaptic pulse (V_{pre} = 0 V, V_{post} = 0.5 V, t_d = 2 ms, V_{drain} = −0.3 V). (C) PPF triggered by a pair of presynaptic pulses (V_{pre} = 0.5 V, V_{post} = 0 V, t_d = 2 ms, Δt = 2 ms). (D) PPD triggered by a pair of presynaptic pulses (V_{pre} = 0 V, V_{post} = 0.5 V, t_d = 2 ms, Δt = 2 ms). (E) EPSC respond to a train of 1 kHz presynaptic pulses (V_{pre} = 0 V, V_{post} = −0.5 V). (F) IPSC respond to a train of 1 kHz presynaptic pulses (V_{pre} = 0 V, V_{post} = 0.5 V). (G) PPD and PPF ratio (A_2/A_1) as a function of spike interval time (Δt).

Synaptic Behavior. Synapses are the connections between the neuron circuits that dominate the architecture of animal brains. Each neuron has over 1000 synapse connections with other neurons. Artificial synapse devices with similar physical properties, such as OECTs, would enable board applications to neuromorphic computing.[55] Modeling of OECT synaptic behaviors is a crucial step toward an improved perspective on synaptic behaviors. The phosphate-buffered saline (PBS) electrolyte with an Au electrode receives a presynaptic input signal (in the form of gate voltage) and passes the signal to the channel. The PEDOT:PSS channel responds to the presynaptic signal and transmits a postsynaptic output signal in the form of a source−drain current (I_{ds}). For our simulation, the amplitude of the presynaptic spike is set to be 0.5 V. V_{pre} = 0, 0.5 V are chosen as input baselines. The choice of these two conditions ensures intense initial doped and de-doped states of polymer, respectively, which leads to better comparison.

When a positive voltage V_{pre} with a duration t_d is applied at the gate electrode, cations in PBS electrolyte (mostly Na^+) are driven to penetrate into the PEDOT:PSS channel and de-dope PEDOT from PSS, therefore lowering the conductance of the channel. In Figure 3B, upon the application of a single positive presynaptic spike with an amplitude of 0.5 V and a duration of 2 ms, the postsynaptic current (PSC) decreases immediately by around 1/3. Because of the positive spike applied, cations in the electrolyte are driven into the polymer channel and compensate for holes in hole/PSS pairs. As a result, originally positively charged PEDOT is reduced, and the channel conductance decreases. This is analogous to IPSC in biological inhibitory synapses. After the removal of the spike, injected cations return to the electrolyte, PEDOT:PSS gets reversibly doped, and PSC gradually recovers to its original state.

In contrast, when a negative presynaptic spike with the same amplitude and duration is applied, PSC is boosted due to cations extracted from polymer while also recovering a little after. This process reproduces EPSC in biological neurons (Figure 3A). Temporally correlated behaviors between presynapse and postsynapse are important as it contains short-term memristive behavior. The process of synaptic facilitation and depression both occur and decay within a short period of time after being simulated. A paired-pulse study is used to analyze the temporal correlation.[56] A pair of pulses with identical amplitude and duration is applied successively with a certain time interval as a presynaptic signal. The resulting postsynaptic current is recorded simultaneously as a function of time. A typical time interval of 2 ms is used to reproduce paired-pulse facilitation (PPF) and paired-pulse depression (PPD). PPF and PPD are forms of short-term synaptic plasticity and are reported to be essential for decoding temporal information in biological systems. Such behaviors can be mimicked by synaptic transistors and thus our simulation.[11] When a pair of negative pulses is applied, since the time interval is short, ions are not completely transported and PEDOT is still relatively highly doped, which results in a stronger second current compared to the first one as in Figure 3C. The second postsynaptic current is facilitated, which means the maximum drain current difference *A* (Figure S4) of the second postsynaptic current (A_2) is greater than that of the first pulse ($A_2/A_1 > 1$). This behavior is analogous to PPF in biological synapses. On the contrary, with a pair of positive pulses applied, the second postsynaptic current is depressed ($A_2/A_1 < 1$) as PPD in biological synapses.[57]

The ratio of A_2/A_1 represents the information processing ability of the synapse.[56] Figure 3G shows the PPD and PPF ratio as a function of spike interval time (Δt). With a longer Δt, the injected ions have more time to return to the electrolyte and the PPD/PPF values increase/decrease exponentially to approach the value of 1 with a critical value

https://doi.org/10.1021/acsomega.1c06864
ACS Omega 2022, 7, 14622−14629

around 40 ms. For Δt longer than the critical value, ions have sufficient time to return and the channel recovers to its original state after the first pulse. The information between spikes is lost and the synaptic OECT runs in the information nonprocessing mode.

The temporal correlation effect was further validated by synaptic facilitation (Figure 3E) and depression (Figure 3F).[58] Both results are produced by applying a 1 kHz train of pulses of an amplitude of 0.5 V. The spike-amplitude-dependent plasticity (SADP) is also a typical postsynaptic behavior of the STP effect. As presented in Figure S6, the value difference between baseline and result PSC (ΔPSC) for IPSC decreases with V_{pre} in a significant linear manner. However, for EPSC, ΔPSC decreases with V_{pre} nonlinearly while approaching zero, as one can predict with increasing gate voltage. The behavior agrees well with previous experimental results. Postsynaptic behavior is further demonstrated by the spike-duration-dependent plasticity (SDDP) (Figure S5); ΔPSC decreases in the IPSC mode but increases in the EPSC mode, both synchronously with duration time t_d. It can be explained by the fact that more cations are injected/extracted in/from the polymer for a longer duration of time of the applied gate voltage. At a certain point when cations can no longer keep injecting/extracting, the system saturates, which leads to the plateau at ∼15 ms for IPSC and ∼28 ms for EPSC.

CONCLUSIONS

We present a robust simulation platform for 2D time-dependent PEDOT:PSS-based OECTs. Applying the concept of phase separation in the semiconductor material and ion injection physics, we are able to reproduce lots of experimental ion transport and charging data of OECTs. Moreover, we demonstrate different typical synaptic phenomena of OECTs under both inhibitory and excitatory modes. Our model is very effective for the simulation of synaptic behaviors of OECTs. At the same time, our platform enables the simulation of tailored OECTs with a fast response speed, high transconductance, and low power consumption, opening a new paradigm for energy-efficient neuromorphic computing platforms. High tunability and applicability to a wide range of semiconductor materials make our platform crucial for developing future organic-based neuromorphic devices.

MATERIALS AND METHODS

Finite-element calculations were carried out with the COMSOL Multiphysics 5.5 software on a standard laptop. Steady-state simulation results were used as input values for time-dependent simulations.

ASSOCIATED CONTENT

Supporting Information

The Supporting Information is available free of charge at https://pubs.acs.org/doi/10.1021/acsomega.1c06864.

Full sets of drift−diffusion equations; boundary conditions; and spike-amplitude-dependent plasticity and spike-duration-dependent plasticity results (PDF)

AUTHOR INFORMATION

Corresponding Author

Xiaoxue Wang − *Department of Chemical and Biomolecular Engineering, The Ohio State University, Columbus, Ohio 43210, United States;* orcid.org/0000-0002-7231-9841; Email: wang.12262@osu.edu

Authors

Haonian Shu − *Department of Chemical and Biomolecular Engineering, The Ohio State University, Columbus, Ohio 43210, United States*

Haowei Long − *School of Materials Science and Engineering, Zhejiang University, Hangzhou, Zhejiang 310027, P. R. China*

Haibin Sun − *Department of Chemical and Biomolecular Engineering, The Ohio State University, Columbus, Ohio 43210, United States*

Baochen Li − *Department of Chemical and Biomolecular Engineering, The Ohio State University, Columbus, Ohio 43210, United States*

Haomiao Zhang − *State Key Laboratory of Chemical Engineering, College of Chemical and Biological Engineering, Zhejiang University, Hangzhou 310027, P. R. China;* orcid.org/0000-0001-7933-3155

Complete contact information is available at: https://pubs.acs.org/10.1021/acsomega.1c06864

Author Contributions

X.W. and H.Shu conceived the project and the physical model. H.Shu and H.L. conducted the COMSOL simulation under the guidance of X.W. and H.Z. H.Shu, H.L., and X.W. prepared the manuscript. H.Sun and B.L. contributed to the discussion of the research ideas and writing of the manuscript. All authors contributed to the manuscript.

Notes

The authors declare no competing financial interest.

Data and materials availability: all data needed to evaluate the conclusions in the paper are present in the paper and/or the Supporting Information. Additional data related to this paper may be requested from the authors.

The authors declare that they have no competing interests.

ACKNOWLEDGMENTS

The authors would like to acknowledge the funding support from the Ohio State University. This work was supported in part by the Ohio State University Materials Research Seed Grant Program, funded by the Center for Emergent Materials, an NSF-MRSEC, grant DMR-2011876, the Center for Exploration of Novel Complex Materials, and the Institute for Materials Research.

REFERENCES

(1) Berggren, K.; Xia, Q.; Likharev, K. K.; Strukov, D. B.; Jiang, H.; Mikolajick, T.; Querlioz, D.; Salinga, M.; Erickson, J. R.; Pi, S.; Xiong, F.; Lin, P.; Li, C.; Chen, Y.; Xiong, S.; Hoskins, B. D.; Daniels, M. W.; Madhavan, A.; Liddle, J. A.; McClelland, J. J.; Yang, Y.; Rupp, J.; Nonnenmann, S. S.; Cheng, K. T.; Gong, N.; Lastras-Montañ, oM. A.; Talin, A. A.; Salleo, A.; Shastri, B. J.; De Lima, T. F.; Prucnal, P.; Tait, A. N.; Shen, Y.; Meng, H.; Roques-Carmes, C.; Cheng, Z.; Bhaskaran, H.; Jariwala, D.; Wang, H.; Shainline, J. M.; Segall, K.; Yang, J. J.; Roy, K.; Datta, S.; Raychowdhury, A. Roadmap on Emerging Hardware and Technology for Machine Learning. *Nanotechnology* **2020**, *32*, No. 012002.

(2) Yu, S. Neuro-Inspired Computing with Emerging Nonvolatile Memorys. *Proc. IEEE* **2018**, *106*, 260−285.

(3) Sebastian, A.; le Gallo, M.; Khaddam-Aljameh, R.; Eleftheriou, E. Memory Devices and Applications for In-Memory Computing. *Nat. Nanotechnol.* **2020**, *15*, 529−544.

(4) Liu, C.; Chen, H.; Hou, X.; Zhang, H.; Han, J.; Jiang, Y. G.; Zeng, X.; Zhang, D. W.; Zhou, P. Small Footprint Transistor Architecture for Photoswitching Logic and in Situ Memory. *Nat. Nanotechnol.* **2019**, *14*, 662−667.
(5) Xu, W.; Min, S. Y.; Hwang, H.; Lee, T. W. Organic Core-Sheath Nanowire Artificial Synapses with Femtojoule Energy Consumption. *Sci. Adv.* **2016**, *2*, No. e1501326.
(6) Ling, H.; Koutsouras, D. A.; Kazemzadeh, S.; van de Burgt, Y.; Yan, F.; Gkoupidenis, P. Electrolyte-Gated Transistors for Synaptic Electronics, Neuromorphic Computing, and Adaptable Biointerfacing. *Appl. Phys. Rev.* **2020**, *7*, No. 011307.
(7) Yang, J. T.; Ge, C.; Du, J. Y.; Huang, H. Y.; He, M.; Wang, C.; Lu, H. B.; Yang, G. Z.; Jin, K. J. Artificial Synapses Emulated by an Electrolyte-Gated Tungsten-Oxide Transistor. *Adv. Mater.* **2018**, *30*, No. 1801548.
(8) Gkoupidenis, P.; Schaefer, N.; Strakosas, X.; Fairfield, J. A.; Malliaras, G. G. Synaptic Plasticity Functions in an Organic Electrochemical Transistor. *Appl. Phys. Lett.* **2015**, *107*, No. 263302.
(9) Ohno, T.; Hasegawa, T.; Tsuruoka, T.; Terabe, K.; Gimzewski, J. K.; Aono, M. Short-Term Plasticity and Long-Term Potentiation Mimicked in Single Inorganic Synapses. *Nat. Mater.* **2011**, *10*, 591−595.
(10) Alibart, F.; Pieutin, S.; Guérin, D.; Novembre, C.; Lenfant, S.; Lmimouni, K.; Gamrat, C.; Vuillaume, D. An Organic Nanoparticle Transistor Behaving as a Biological Spiking Synapse. *Adv. Funct. Mater.* **2010**, *20*, 330−337.
(11) Zhu, L. Q.; Wan, C. J.; Guo, L. Q.; Shi, Y.; Wan, Q. Artificial Synapse Network on Inorganic Proton Conductor for Neuromorphic Systems. *Nat. Commun.* **2014**, *5*, No. 3158.
(12) Sokolov, A. S.; Ali, M.; Riaz, R.; Abbas, Y.; Ko, M. J.; Choi, C. Silver-Adapted Diffusive Memristor Based on Organic Nitrogen-Doped Graphene Oxide Quantum Dots (N-GOQDs) for Artificial Biosynapse Applications. *Adv. Funct. Mater.* **2019**, *29*, No. 1807504.
(13) Wang, Y.; Lv, Z.; Chen, J.; Wang, Z.; Zhou, Y.; Zhou, L.; Chen, X.; Han, S. T. Photonic Synapses Based on Inorganic Perovskite Quantum Dots for Neuromorphic Computing. *Adv. Mater.* **2018**, *30*, No. 1802883.
(14) Zhu, Q. B.; Li, B.; Yang, D. D.; Liu, C.; Feng, S.; Chen, M. L.; Sun, Y.; Tian, Y. N.; Su, X.; Wang, X. M.; Qiu, S.; Li, Q. W.; Li, X. M.; Zeng, H. B.; Cheng, H. M.; Sun, D. M. A Flexible Ultrasensitive Optoelectronic Sensor Array for Neuromorphic Vision Systems. *Nat. Commun.* **2021**, *12*, No. 1798.
(15) Ham, S.; Kang, M.; Jang, S.; Jang, J.; Choi, S.; Kim, T. W.; Wang, G. One-Dimensional Organic Artificial Multi-Synapses Enabling Electronic Textile Neural Network for Wearable Neuromorphic Applications. *Sci. Adv.* **2020**, *6*, 1−10.
(16) Milano, G.; Luebben, M.; Ma, Z.; Dunin-Borkowski, R.; Boarino, L.; Pirri, C. F.; Waser, R.; Ricciardi, C.; Valov, I. Self-Limited Single Nanowire Systems Combining All-in-One Memristive and Neuromorphic Functionalities. *Nat. Commun.* **2018**, *9*, No. 5151.
(17) Zhou, G.; Sun, B.; Ren, Z.; Wang, L.; Xu, C.; Wu, B.; Li, P.; Yao, Y.; Duan, S. Resistive Switching Behaviors and Memory Logic Functions in Single MnOx Nanorod Modulated by Moisture. *Chem. Commun.* **2019**, *55*, 9915−9918.
(18) Kim, K.; Chen, C. L.; Truong, Q.; Shen, A. M.; Chen, Y. A Carbon Nanotube Synapse with Dynamic Logic and Learning. *Adv. Mater.* **2013**, *25*, 1693−1698.
(19) Cao, G.; Meng, P.; Chen, J.; Liu, H.; Bian, R.; Zhu, C.; Liu, F.; Liu, Z. 2D Material Based Synaptic Devices for Neuromorphic Computing. *Adv. Funct. Mater.* **2021**, *31*, No. 2005443.
(20) Jiang, J.; Guo, J.; Wan, X.; Yang, Y.; Xie, H.; Niu, D.; Yang, J.; He, J.; Gao, Y.; Wan, Q. 2D MoS2 Neuromorphic Devices for Brain-Like Computational Systems. *Small* **2017**, *13*, No. 1700933.
(21) Zhu, X.; Li, D.; Liang, X.; Lu, W. D. Ionic Modulation and Ionic Coupling Effects in MoS 2 Devices for Neuromorphic Computing. *Nat. Mater.* **2019**, *18*, 141−148.
(22) Sangwan, V. K.; Lee, H. S.; Bergeron, H.; Balla, I.; Beck, M. E.; Chen, K. S.; Hersam, M. C. Multi-Terminal Memtransistors from Polycrystalline Monolayer Molybdenum Disulfide. *Nature* **2018**, *554*, 500−504.
(23) Li, H.; Jiang, X.; Ye, W.; Zhang, H.; Zhou, L.; Zhang, F.; She, D.; Zhou, Y.; Han, S. T. Fully Photon Modulated Heterostructure for Neuromorphic Computing. *Nano Energy* **2019**, *65*, No. 104000.
(24) Sangwan, V. K.; Hersam, M. C. Neuromorphic Nanoelectronic Materials. *Nat. Nanotechnol.* **2020**, *15*, 517−528.
(25) Wang, T. Y.; Meng, J. L.; Rao, M. Y.; He, Z. Y.; Chen, L.; Zhu, H.; Sun, Q. Q.; Ding, S. J.; Bao, W. Z.; Zhou, P.; Zhang, D. W. Three-Dimensional Nanoscale Flexible Memristor Networks with Ultralow Power for Information Transmission and Processing Application. *Nano Lett.* **2020**, *20*, 4111−4120.
(26) Ryu, J. H.; Mahata, C.; Kim, S. Long-Term and Short-Term Plasticity of Ta2O5/HfO2 Memristor for Hardware Neuromorphic Application. *J. Alloys Compd.* **2021**, *850*, No. 156675.
(27) Li, J.; Ge, C.; Du, J.; Wang, C.; Yang, G.; Jin, K. Reproducible Ultrathin Ferroelectric Domain Switching for High-Performance Neuromorphic Computing. *Adv. Mater.* **2020**, *32*, No. 1905764.
(28) Liu, R.; Ulbrandt, J. G.; Hsing, H. C.; Gura, A.; Bein, B.; Sun, A.; Pan, C.; Bertino, G.; Lai, A.; Cheng, K.; Doyle, E.; Evans-Lutterodt, K.; Headrick, R. L.; Dawber, M. Role of Ferroelectric Polarization during Growth of Highly Strained Ferroelectric Materials. *Nat. Commun.* **2020**, *11*, No. 2630.
(29) Yeon, H.; Lin, P.; Choi, C.; Tan, S. H.; Park, Y.; Lee, D.; Lee, J.; Xu, F.; Gao, B.; Wu, H.; Qian, H.; Nie, Y.; Kim, S.; Kim, J. Alloying Conducting Channels for Reliable Neuromorphic Computing. *Nat. Nanotechnol.* **2020**, *15*, 574−579.
(30) Xie, D.; Wei, L.; Xie, M.; Jiang, L.; Yang, J.; He, J.; Jiang, J. Photoelectric Visual Adaptation Based on 0D-CsPbBr3-Quantum-Dots/2D-MoS2 Mixed-Dimensional Heterojunction Transistor. *Adv. Funct. Mater.* **2021**, *31*, No. 2010655.
(31) Cheng, Y.; Li, H.; Liu, B.; Jiang, L.; Liu, M.; Huang, H.; Yang, J.; He, J.; Jiang, J. Vertical 0D-Perovskite/2D-MoS2 van Der Waals Heterojunction Phototransistor for Emulating Photoelectric-Synergistically Classical Pavlovian Conditioning and Neural Coding Dynamics. *Small* **2020**, *16*, No. 2005217.
(32) Cheng, Y.; Shan, K.; Xu, Y.; Yang, J.; He, J.; Jiang, J. Hardware Implementation of Photoelectrically Modulated Dendritic Arithmetic and Spike-Timing-Dependent Plasticity Enabled by an Ion-Coupling Gate-Tunable Vertical 0D-Perovskite/2D-MoS2hybrid-Dimensional van Der Waals Heterostructure. *Nanoscale* **2020**, *12*, 21798−21811.
(33) Feng, G.; Jiang, J.; Li, Y.; Xie, D.; Tian, B.; Wan, Q. Flexible Vertical Photogating Transistor Network with an Ultrashort Channel for In-Sensor Visual Nociceptor. *Adv. Funct. Mater.* **2021**, *31*, No. 2104327.
(34) Feng, G.; Jiang, J.; Zhao, Y.; Wang, S.; Liu, B.; Yin, K.; Niu, D.; Li, X.; Chen, Y.; Duan, H.; Yang, J.; He, J.; Gao, Y.; Wan, Q. A Sub-10 Nm Vertical Organic/Inorganic Hybrid Transistor for Pain-Perceptual and Sensitization-Regulated Nociceptor Emulation. *Adv. Mater.* **2020**, *32*, No. 1906171.
(35) Faria, G. C.; Duong, D. T.; Salleo, A. On the Transient Response of Organic Electrochemical Transistors. *Org. Electron.* **2017**, *45*, 215−221.
(36) Khodagholy, D.; Rivnay, J.; Sessolo, M.; Gurfinkel, M.; Leleux, P.; Jimison, L. H.; Stavrinidou, E.; Herve, T.; Sanaur, S.; Owens, R. M.; Malliaras, G. G. High Transconductance Organic Electrochemical Transistors. *Nat. Commun.* **2013**, *4*, No. 2133.
(37) Rivnay, J.; Leleux, P.; Ferro, M.; Sessolo, M.; Williamson, A.; Koutsouras, D. A.; Khodagholy, D.; Ramuz, M.; Strakosas, X.; Owens, R. M.; Benar, C.; Badier, J. M.; Bernard, C.; Malliaras, G. G. High-Performance Transistors for Bioelectronics through Tuning of Channel Thickness. *Sci. Adv.* **2015**, *1*, No. e1400251.
(38) Van De Burgt, Y.; Lubberman, E.; Fuller, E. J.; Keene, S. T.; Faria, G. C.; Agarwal, S.; Marinella, M. J.; Alec Talin, A.; Salleo, A. A Non-Volatile Organic Electrochemical Device as a Low-Voltage Artificial Synapse for Neuromorphic Computing. *Nat. Mater.* **2017**, *16*, 414−418.
(39) Gerasimov, J. Y.; Gabrielsson, R.; Forchheimer, R.; Stavrinidou, E.; Simon, D. T.; Berggren, M.; Fabiano, S. An Evolvable Organic

https://doi.org/10.1021/acsomega.1c06864
ACS Omega 2022, 7, 14622−14629

Electrochemical Transistor for Neuromorphic Applications. *Adv. Sci.* **2019**, *6*, No. 1801339.
(40) Gkoupidenis, P.; Koutsouras, D. A.; Malliaras, G. G. Neuromorphic Device Architectures with Global Connectivity through Electrolyte Gating. *Nat. Commun.* **2017**, *8*, No. 15448.
(41) Rivnay, J.; Inal, S.; Salleo, A.; Owens, R. M.; Berggren, M.; Malliaras, G. G. Organic Electrochemical Transistors. *Nat. Rev. Mater.* **2018**, *3*, No. 17086.
(42) Alamo, J. A. *Integrated Microelectronics Devices*; Pearson, 2017.
(43) Shirinskaya, A.; Horowitz, G.; Rivnay, J.; Malliaras, G. G.; Bonnassieux, Y. T. *Biosensors* **2018**, *8*, No. 103.
(44) Tybrandt, K.; Zozoulenko, I. V.; Berggren, M. Chemical Potential-Electric Double Layer Coupling in Conjugated Polymer-Polyelectrolyte Blends. *Sci. Adv.* **2017**, *3*, No. eaao3659.
(45) Volkov, A. V.; Wijeratne, K.; Mitraka, E.; Ail, U.; Zhao, D.; Tybrandt, K.; Andreasen, J. W.; Berggren, M.; Crispin, X.; Zozoulenko, I. V. Understanding the Capacitance of PEDOT:PSS. *Adv. Funct. Mater.* **2017**, *27*, No. 1700329.
(46) Sharma, A.; Sheinman, M. Analytical Approximation for Chemical Potential in Organic Materials with Gaussian Density of States. *J. Phys. D: Appl. Phys.* **2013**, *46*, No. 125106.
(47) Friedlein, J. T.; Rivnay, J.; Dunlap, D. H.; McCulloch, I.; Shaheen, S. E.; McLeod, R. R.; Malliaras, G. G. Influence of Disorder on Transfer Characteristics of Organic Electrochemical Transistors. *Appl. Phys. Lett.* **2017**, *111*, No. 023301.
(48) Ambegaokar, V.; Halperin, B. I.; Langer, J. S. Hopping Conductivity in Disordered Systems. *Phys. Rev. B* **1971**, *4*, 2612−2620.
(49) Bisquert, J.; Fabregat-Santiago, F.; Mora-Seró, I.; Garcia-Belmonte, G.; Barea, E. M.; Palomares, E. A Review of Recent Results on Electrochemical Determination of the Density of Electronic States of Nanostructured Metal-Oxide Semiconductors and Organic Hole Conductors. *Inorg. Chim. Acta* **2008**, *361*, 684−698.
(50) Bernards, D. A.; Malliaras, G. G. Steady-State and Transient Behavior of Organic Electrochemical Transistors. *Adv. Funct. Mater.* **2007**, *17*, 3538−3544.
(51) Paulsen, B. D.; Tybrandt, K.; Stavrinidou, E.; Rivnay, J. Organic Mixed Ionic−Electronic Conductors. *Nat. Mater.* **2020**, *19*, 13−26.
(52) Wang, X.; Zhang, X.; Sun, L.; Lee, D.; Lee, S.; Wang, M.; Zhao, J.; Shao-Horn, Y.; Dincă, M.; Palacios, T.; Gleason, K. K. High Electrical Conductivity and Carrier Mobility in OCVD PEDOT Thin Films by Engineered Crystallization and Acid Treatment. *Sci. Adv.* **2018**, *4*, No. eaat5780.
(53) Friedlein, J. T.; McLeod, R. R.; Rivnay, J. Device Physics of Organic Electrochemical Transistors. *Org. Electron.* **2018**, *63*, 398−414.
(54) Kaphle, V.; Liu, S.; Al-Shadeedi, A.; Keum, C. M.; Lüssem, B. Contact Resistance Effects in Highly Doped Organic Electrochemical Transistors. *Adv. Mater.* **2016**, *28*, 8766−8770.
(55) Wang, Z.; Joshi, S.; Savel'ev, S. E.; Jiang, H.; Midya, R.; Lin, P.; Hu, M.; Ge, N.; Strachan, J. P.; Li, Z.; Wu, Q.; Barnell, M.; Li, G. L.; Xin, H. L.; Williams, R. S.; Xia, Q.; Yang, J. J. Memristors with Diffusive Dynamics as Synaptic Emulators for Neuromorphic Computing. *Nat. Mater.* **2017**, *16*, 101−108.
(56) Ling, H.; Wang, N.; Yang, A.; Liu, Y.; Song, J.; Yan, F. Dynamically Reconfigurable Short-Term Synapse with Millivolt Stimulus Resolution Based on Organic Electrochemical Transistors. *Adv. Mater. Technol.* **2019**, *4*, No. 1900471.
(57) Gkoupidenis, P.; Schaefer, N.; Garlan, B.; Malliaras, G. G. Neuromorphic Functions in PEDOT:PSS Organic Electrochemical Transistors. *Adv. Mater.* **2015**, *27*, 7176−7180.
(58) Jackman, S. L.; Regehr, W. G. The Mechanisms and Functions of Synaptic Facilitation. *Neuron* **2017**, *94*, 447−464.

https://doi.org/10.1021/acsomega.1c06864
ACS Omega 2022, 7, 14622−14629